



Sulfate radical-based photo-Fenton reaction derived by CuBi₂O₄ and its composites with α-Bi₂O₃ under visible light irradiation: Catalyst fabrication, performance and reaction mechanism



Yiping Wang^a, Chao Liu^a, Yuting Zhang^a, Weidong Meng^a, Bin Yu^b, Shengyan Pu^c, Donghai Yuan^d, Fei Qi^{a,*}, Bingbing Xu^{e,**}, Wei Chu^f

^a Beijing Key Lab for Source Control Technology of Water Pollution, College of Environmental Science and Engineering, Beijing Forestry University, Beijing, 100083, PR China

^b Poten Environmental Engineering Co., Ltd., Beijing, 100082, PR China

^c State Key Laboratory of Geohazard Prevention and Geoenvironment Protection, Chengdu University of Technology, Chengdu, 610059, PR China

^d Key Laboratory of Urban Stormwater System and Water Environment, Ministry of Education, Beijing University of Civil Engineering and Architecture, Beijing, 100044, PR China

^e State Key Laboratory of Environmental Criteria and Risk Assessment, Chinese Research Academy of Environmental Sciences, Beijing, 100012, PR China

^f Department of Civil and Environmental Engineering, The Hong Kong Polytechnic University, Hung Hom, Kowloon, Hong Kong

ARTICLE INFO

Keywords:

CuBi₂O₄
Sulfate radical photo-Fenton
Rhodamine B
Peroxymonosulfate

ABSTRACT

Sulfate radical-based photo-Fenton (SR-photo-Fenton) reaction, assisted by visible light irradiation, was achieved by CuBi₂O₄ and its composites with α-Bi₂O₃ for refractory chemical degradation in aqueous solution. Herein, this catalyst was fabricated by a sol-gel method and the fabrication conditions, including calcination temperature and molar ratio of Cu/Bi, were optimized according to the crystal phase composition, catalytic activity and toxic copper ion leaching. The optimal calcination temperature was 500 °C and molar ratio of Bi to Cu was 2.0. The catalyst containing CuBi₂O₄ and α-Bi₂O₃ showed a higher density of surface –OH which might be the key surface active site than pure CuBi₂O₄. The influence of initial solution pH, PMS concentration, catalyst dosage and catalyst reuse on rhodamine B (RhB) degradation was investigated. Importantly, calcination at 500 °C reverted the catalytic activity of catalyst. Results of electron paramagnetic resonance, competitive radical experiments and surface chemical property characterization demonstrated that the reaction mechanism of this novel SR-photo-Fenton reaction is a combination of interface and solution reactions. In the interface reaction, the transfer of photogenerated electron/hole pairs drives the decomposition of PMS to produce SO₄^{·-} and ·OH. Furthermore, the cycling of Cu(I)/Cu(II) facilitated effective PMS activation to generate free radical that was responsible for the degradation of RhB. The second order reaction rate constant between RhB and SO₄^{·-} was determined to be 0.595–6.436 × 10¹⁰ M⁻¹ S⁻¹ based on the chemical reaction kinetics of radical, which was a first and important report for SO₄^{·-} chemistry.

1. Introduction

In recent years, hybrid advanced oxidation processes (AOPs) derived from heterogeneous activation of peroxymonosulfate (PMS) and other AOPs such as ultrasonic irradiation [1], UV-vis irradiation, ozonation [2] and microwave irradiation [3], have received considerable attention [4]. These processes feature high degradation performance of refractory organic contaminants, improved utilization efficiency of PMS, and enhanced formation of sulfate radical (SO₄^{·-}). Sulfate radical-based photo-Fenton (SR-photo-Fenton) reactions, consisting of

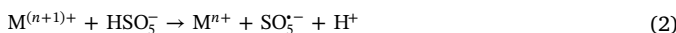
visible light irradiation and activation of PMS, are a widely studied type of hybrid AOP. To develop the applicability of SR-photo-Fenton, heterogeneous reactions are desirable. Among the catalysts used in SR-photo-Fenton, some show bifunctional performance on both activation PMS and photocatalysis, such as Co-doped TiO₂ [5], BiVO₄ [6], Ag/mpg-C₃N₄ [7], g-C₃N₄-INA-FePcC₁₆ [8]. However, some catalysts only improve the efficiency of the PMS activation, assisted by light irritation, such as MFe₂O₄ (M = Cu, Zn, Ni, and Co) [9]. In SR-photo-Fenton reactions, PMS is not only an oxidant activated by the catalyst to generate reactive radicals (SO₄^{·-} and ·OH et al.) (Eqs. (1) and (2)) but also an

* Corresponding author.

** Corresponding author.

E-mail addresses: qifei@bjfu.edu.cn, qifei_hit@163.com (F. Qi), xbb_hit@126.com (B. Xu).

electron acceptor that can decrease the recombination of photo-generated electrons (e^-) and holes (h^+) [5]. The h^+ reacts with PMS to produce SO_4^{2-} , as Eqs. (3) and (4) [10]. The formed e^- is able to decompose PMS to produce SO_4^{2-} and $\cdot\text{OH}$ (Eqs. (5) and (6)) [11], increasing the degradation performance of the refractory organic contaminants. Additionally, PMS can be activated in the presence of visible light, producing SO_4^{2-} and $\cdot\text{OH}$ (Eq. (7)). The photogenerated e^- can also regenerate active transition metal ions (i.e., Co^{3+} to Co^{2+}) by transferring it to the transition metal [5]. The synergistic effects in SR-photo-Fenton reactions show great promise for future applications in water purification; however, the development of more efficient and stable catalysts for SR-photo-Fenton processes is required.



CuBi_2O_4 is a p-type semiconductor, which shows excellent visible light absorption properties [12] but lacks photocatalytic activity owing to its high photostability and rapid recombination of e^- and h^+ [13]. However, the photocatalytic activity of CuBi_2O_4 can be enhanced through the formation of a heterojunction with Ag_3PO_4 [14], WO_3 [15], BiVO_4 [15–17], reduced graphene oxide [18], MWCNTs [19], and TiO_2 [20]. The addition of H_2O_2 is an alternative method of avoiding the recombination of e^- and h^+ , and improving the degradation refractory organic compounds, as a traditional photo-Fenton [13,21]. Additionally, CuBi_2O_4 has been reported to be an efficient catalyst for PMS activation [22–25]. However, some problems still remained, such as the low catalytic activity of pure CuBi_2O_4 and the need for a high concentration of PMS with a molar ratio of [PMS]/[target contaminant] in the range of 15.67–108.14. In addition, copper ion leaching occurs in the range of 12.0–144 $\mu\text{g/g}$ [22,26].

Herein, CuBi_2O_4 and its composites with $\alpha\text{-Bi}_2\text{O}_3$ and CuO were prepared by a sol-gel method, which is much simpler than corresponding hydrothermal processes. As-prepared samples were used in SR-photo-Fenton reaction for rhodamine B (RhB) degradation. The effects of calcination temperature and molar ratio of Cu/Bi in precursors on the crystal phase composition, morphology, interfacial chemical properties, and RhB degradation performance were investigated. The catalytic activity of the optimized catalyst and its metal ion leaching were systematically evaluated. Additionally, effects of initial pH, PMS concentration, catalyst dosage and recycling performance were evaluated, respectively. Regeneration method of the catalyst was provided and variations of the N-de-ethylated degradation intermediates of RhB were quantified. Furthermore, reaction mechanism based on the results of competitive radical and electron paramagnetic resonance (EPR) experiments.

2. Experimental

2.1. Chemicals

$\text{Bi}(\text{NO}_3)_3 \cdot 5\text{H}_2\text{O}$ (> 99.0%), $\text{Cu}(\text{NO}_3)_2 \cdot 3\text{H}_2\text{O}$ (> 99.0%), citric acid monohydrate (> 99.5%), edetate disodium (EDTA-2Na) and RhB (97.5%) were purchased from Sinopharm Chemical Reagent Co., Ltd. Ethanol (> 99.7%) *tert*-butyl alcohol (> 99.0%) and chloroform (> 99.0%) were purchased from Beijing Chemical Works. Oxone® ($2\text{KHSO}_5 \cdot \text{KHSO}_4 \cdot 2\text{K}_2\text{SO}_4$) was obtained from Alfa Aesar. 5,5-Dimethyl-

Table 1
Phase composition and BET of samples.

Effect of calcination temperature on crystal phase composition and BET

Calcination temperature	Name	Phase composition			BET(m^2/g)
		CuBi_2O_4	Bi_2O_3	$\text{Bi}_2\text{O}_2\text{CO}_3$	
300 °C	C1B2O-3	0	84.0%	16.0%	3.3
400 °C	C1B2O-4	54.4%	45.5%	0	5.7
500 °C	C1B2O-5	64.9%	35.1%	0	3.5
600 °C	C1B2O-6	70.6%	29.4%	0	2.5
700 °C	C1B2O-7 (CuBi_2O_4)	100%	0	0	1.3

Effect of mole ratio of Cu and Bi on crystal phase composition

Cu:Bi	Name	Phase composition			BET(m^2/g)
		CuBi_2O_4	Bi_2O_3	CuO	
1:3	C1B3O-5	49.0%	51.0%	0	3.4
1:5	C1B5O-5	30.8%	69.2%	0	2.9
1:10	C1B10O-5	10.6%	89.4%	0	1.9
1:15	C1B15O-5	8.5%	91.5%	0	2.2
1:1	C1B1O-5	65.6 %	0	34.4%	4.0
3:1	C3B1O-5	54.3%	0	45.7%	6.0
5:1	C5B1O-5	42.8%	0	57.2%	7.2
10:1	C10B1O-5	31.3%	0	68.7%	10.5

1-pyrroline (DMPO, > 99.0%) was obtained from J&K Scientific. The methanol used as an eluent for HPLC analysis was provided by J. T. Baker Inc. All chemicals were of reagent grade and used without further purification.

2.2. Preparation and characterization

The CuBi_2O_4 and its composites with $\alpha\text{-Bi}_2\text{O}_3$ or CuO were prepared via a sol-gel method. A certain amount of $\text{Bi}(\text{NO}_3)_3 \cdot 5\text{H}_2\text{O}$ and $\text{Cu}(\text{NO}_3)_2 \cdot 3\text{H}_2\text{O}$ were dissolved in nitric acid solution (10%, 20 mL) under magnetic stirring to obtain a well-dissolved solution. Citric acid monohydrate was added into the aforementioned solution as a complexing agent at a citric acid/ $(\text{Bi}^{3+} + \text{Cu}^{2+})$ molar ratio of 1.2:1. The beaker containing the solution was evaporated in a water bath at 75 °C to obtain a gel, which was dried at 90 °C until a dried solid precursor was obtained. The ground precursor power was annealed for 5 h at different temperatures in a muffle oven at a heating rate of 2 °C/min. The names of as-prepared samples under different conditions are shown in Table 1. Pure CuO and $\alpha\text{-Bi}_2\text{O}_3$ were also prepared by the above method with the addition of $\text{Cu}(\text{NO}_3)_2 \cdot 3\text{H}_2\text{O}$ or $\text{Bi}(\text{NO}_3)_3 \cdot 5\text{H}_2\text{O}$ as precursors, respectively. These samples were calcined at 500 °C for 5 h. The obtained catalyst samples were characterized by X-ray diffraction (XRD), thermogravimetric differential thermal analysis (TG-DTA), Fourier transform infrared (FT-IR) spectroscopy, field emission scanning electron microscopy (FESEM), high-resolution transmission electron microscopy (HRTEM), X-ray photoelectron spectroscopy (XPS), Brunauer–Emmett–Teller (BET) surface area analysis and pH_{pzc} , as described in the Supplementary information (Text S1).

2.3. Experimental procedure for SR-photo-Fenton reaction

Degradation experiments were performed in a constant temperature reactor containing 250 mL of 25 mg/L RhB dye solution, under visible light irradiation from a 300 W xenon lamp with an UV cut-off filter ($\lambda \geq 420 \text{ nm}$). Details of the reaction procedure and analysis methods involved can be found in Text S2.

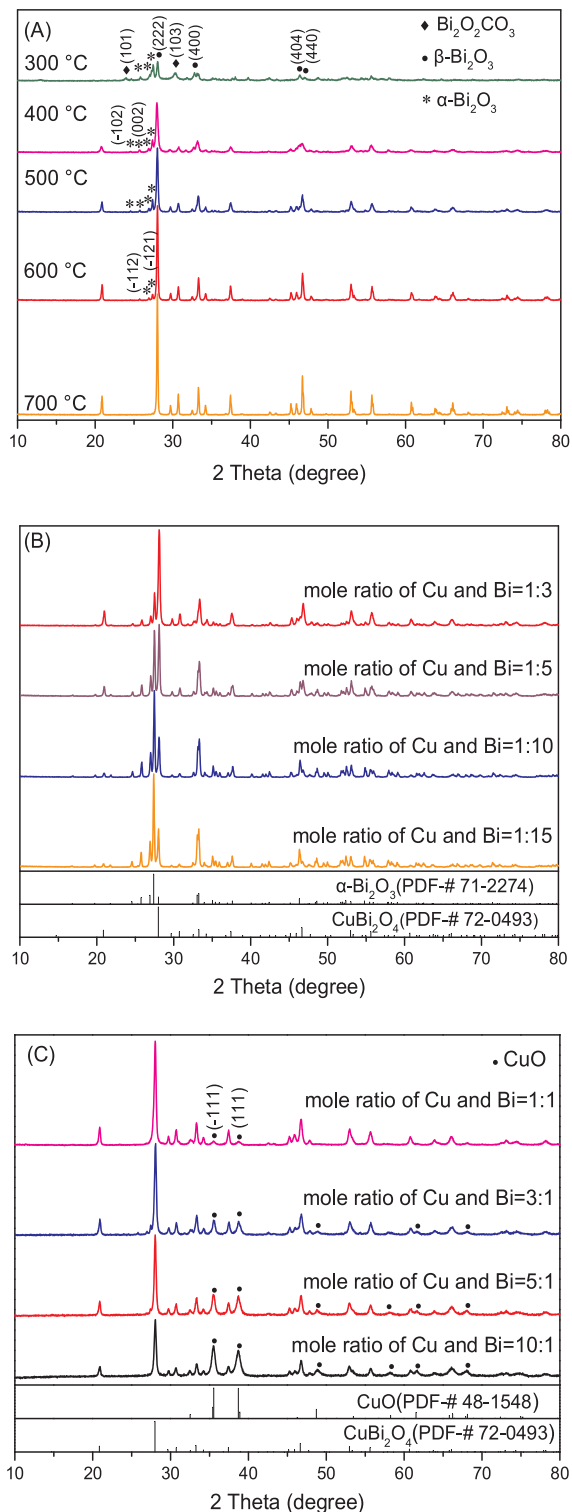


Fig. 1. XRD patterns of samples prepared under (A) different calcination temperature (B) excess bismuth dose (C) excess copper dose.

3. Results and discussion

3.1. Characterization of prepared samples

The effects of calcination temperature (300–700 °C) on the crystal phase of as-prepared samples are shown in Fig. 1(A). When the precursor was annealed at 300 °C (C1B2O-3), a composite of α-Bi₂O₃ (JCPDS 71-2274), β-Bi₂O₃ (JCPDS 78-1793) and Bi₂O₂CO₃ (JCPDS 84-

1752) was formed, without any crystal phases containing copper. The CuBi₂O₄ phase formed at calcination temperatures higher than 400 °C. However, α-Bi₂O₃ was formed as an impurity, as has been previously reported [27]. As the calcination temperature increased further, the content of CuBi₂O₄ increased and that of α-Bi₂O₃ decreased accordingly (Table 1). A single phase of CuBi₂O₄ was formed under calcination at 700 °C (C1B2O-7), all reflection peaks were in good agreement with the tetragonal crystal structure CuBi₂O₄ (JCPDS 72-0493) and no impurities were detected. Furthermore, as the calcination temperature increased, the crystallinity of the samples improved. TG-DTA analysis and FT-IR measurements were performed to study the decomposition mechanism of the precursor (Figs. S1 and S2, Text S3 and S4). It was concluded that calcination temperature required for the decomposition of nitrate and citric acid must be higher than 500 °C.

The effects of the molar ratio of copper and bismuth on the composition of the obtained sample were investigated under the calcination at 500 °C. A combination of α-Bi₂O₃ and CuBi₂O₄ was formed under all conditions with an excess bismuth (Fig. 1(B)). As the bismuth content increased, the intensity of the characteristic diffraction peak of α-Bi₂O₃ at 2θ = 27.4°, which belongs to the (T21) crystal face, was considerable enhanced. Accordingly, the content of α-Bi₂O₃ in the composites increased as the amount of bismuth increased (Table 1). However, owing to the volatilization of bismuth at high temperature, the content of α-Bi₂O₃ in the composite was lower than the theoretical value calculated according to the amount of added bismuth, as listed in Table 1. The excess copper in the precursor led to the formation of CuO and CuBi₂O₄ (Fig. 1(C)). Diffraction peaks of CuO (JCPDS 48-1548) with a monoclinic crystal structure were identified. The intensity of the diffraction peaks of CuO gradually strengthened; however, the characteristic diffraction peak of CuBi₂O₄ at 2θ = 28.02° weakened as the copper dose increased. Similarly, CuO/CuBi₂O₄ and α-Bi₂O₃/CuBi₂O₄ were prepared by solution combustion synthesis with non-stoichiometric Cu:Bi for hydrogen evolution and CO₂ photo-reduction [28]. CuBi₂O₄ was also synthesized by a sol-gel method with acetone and glycerol as complexing agents [29]. This synthesis was complicated and used more harmful chemicals compared with our method based on citric acid. Previous reports on samples prepared by sol-gel method showed irregular messy agglomerate morphology [28,29]. Herein, the morphology of the obtained solid composites was influenced by the calcination temperature and molar ratio of Cu/Bi in the precursor, as shown in Figs. S3, S4 and Text S5.

The HRTEM images (Fig. 2) clearly showed lattice fringes of 0.27 nm, which were ascribed to the (310) plane of CuBi₂O₄ in all showed samples [13]. Lattice fringes of 0.33 nm corresponded to the (111) plane of α-Bi₂O₃ in C1B2O-5 and C1B3O-5 [30], and lattice fringes of 0.23 nm corresponded to the (111) plane of CuO in C3B1O-5 [31]. The results of HRTEM images were consistent with the XRD data. Different calcination temperatures and non-stoichiometric synthesis conditions led to the variation of the specific surface area. The specific surface area of the as-prepared samples was very small and decreased with increasing calcination temperature (Table 1), except for the sample calcined under 300 °C. The specific surface area of CuBi₂O₄ was slightly lower than that prepared by hydrothermal method (3.1–35.2 m² g⁻¹) in previous reports [13,22]. The BET surface area was improved as the copper content increased. This result indicated that the formation of CuO led to an increase of the surface area.

XPS survey spectra (Fig. 3(A)) revealed that Cu, Bi, O, and adventitious C coexisted in the obtained samples. Fig. 3(B) shows XPS spectra of the Cu 2p, peak corresponding to Cu 2p_{1/2} was observed at 955.5 eV with a satellite at 964.9 eV. The Cu 2p_{3/2} peak could be deconvoluted into two peaks at 935.7 and 932.8 eV, which were attributed to Cu²⁺ and reduced copper species, respectively [32,33]. Reduced copper species were further identified by Auger electron spectroscopy (AES) (Fig. S5) and the peak at 912.1 eV in the AES confirmed the existence of Cu⁺. The presence of a small amount of Cu⁺ on the sample's surface might be attributed to the reduction of Cu²⁺ by

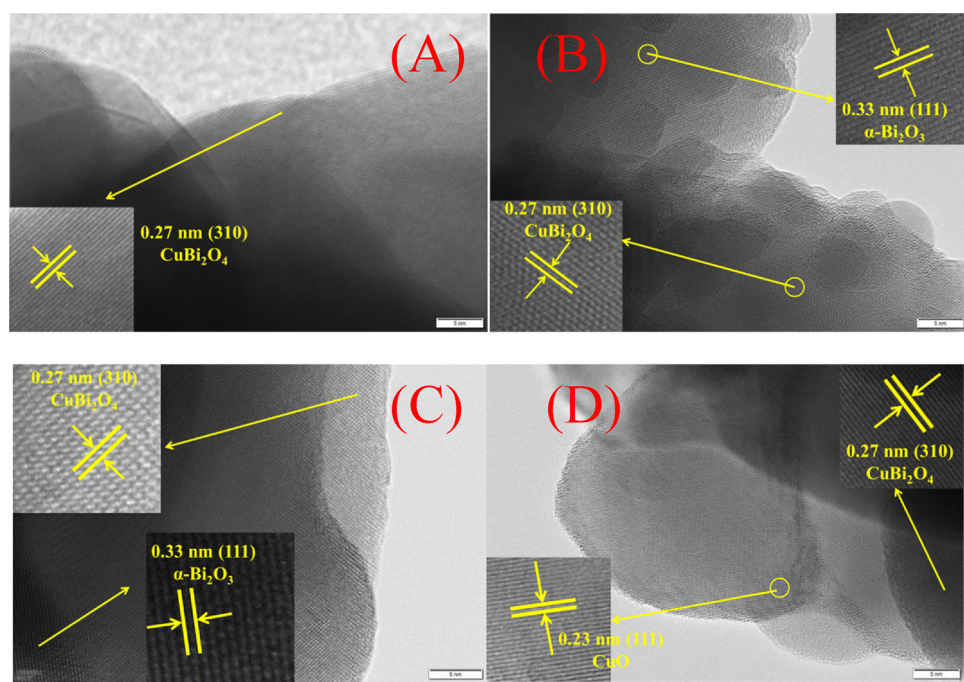


Fig. 2. TEM images of (A) C1B2O-7; (B) C1B2O-5; (C) C1B3O-5; (D) C3B1O-5.

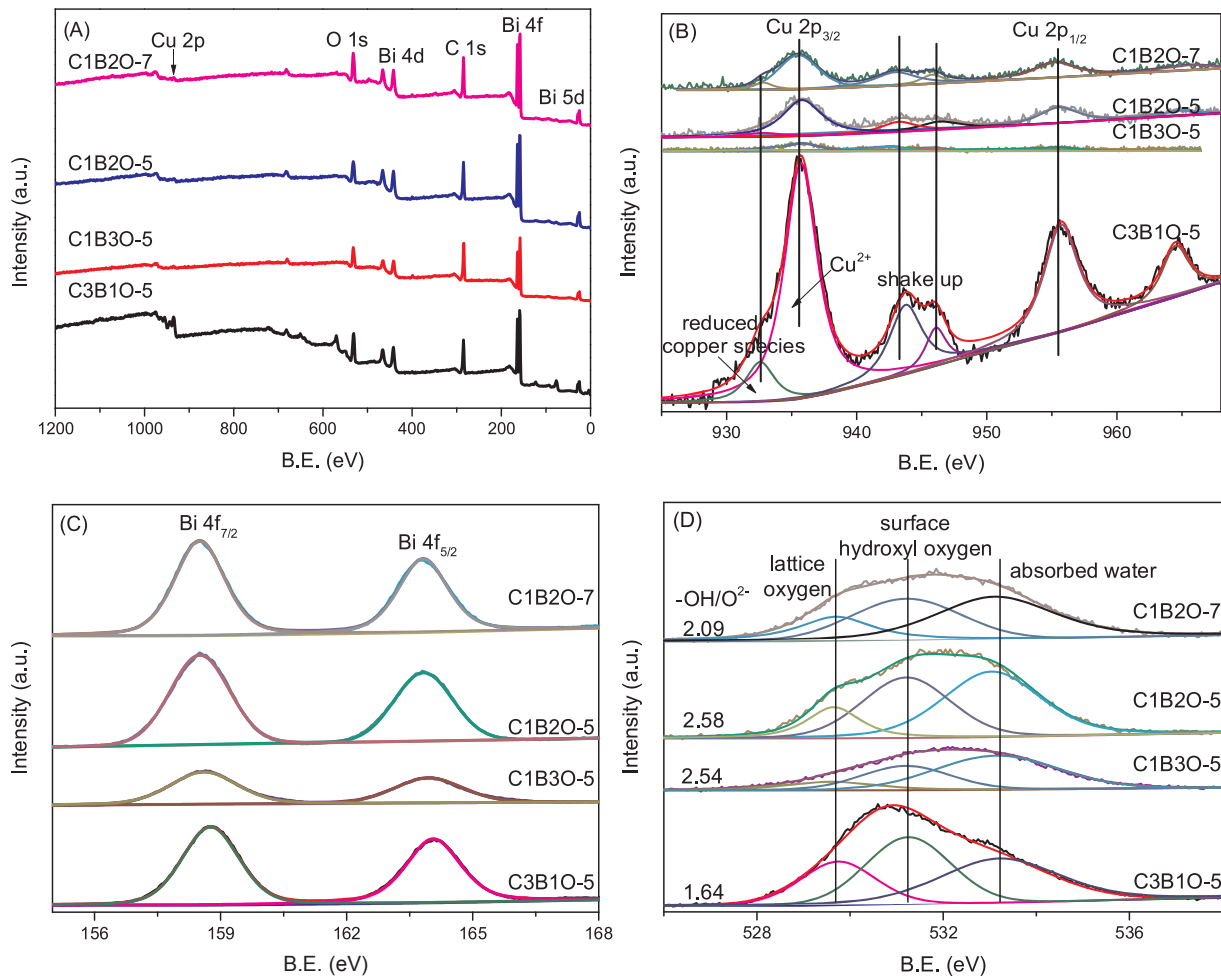


Fig. 3. XPS spectra of sample (A) survey, (B) Cu 2p, (C) Bi 4f and (D) O 1s.

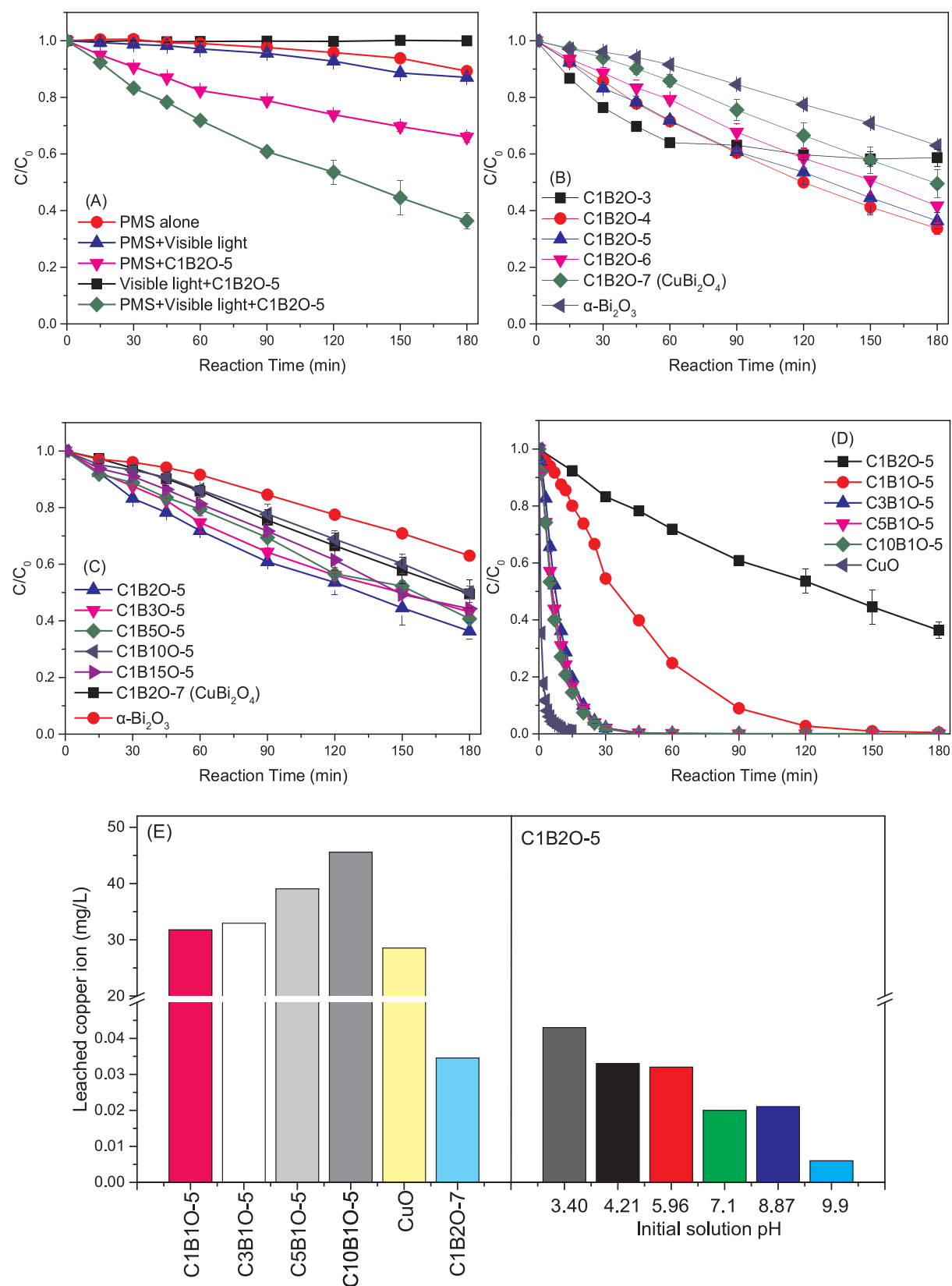


Fig. 4. Degradation of RhB in SR-photo-Fenton with as prepared composite (A) effect of different reaction on RhB degradation; (B) effect of catalyst calcination temperature; (C) effect molar ratio of copper and bismuth as bismuth is excessed; (D) effect molar ratio of copper and bismuth as copper is excessed; (E) leached copper ions with different catalyst and under different initial solution pH.

Reaction condition: [RhB] = 25 mg/L, [PMS] = 0.65 mM, [catalyst] = 0.8 g/L, and pH = 3.4.

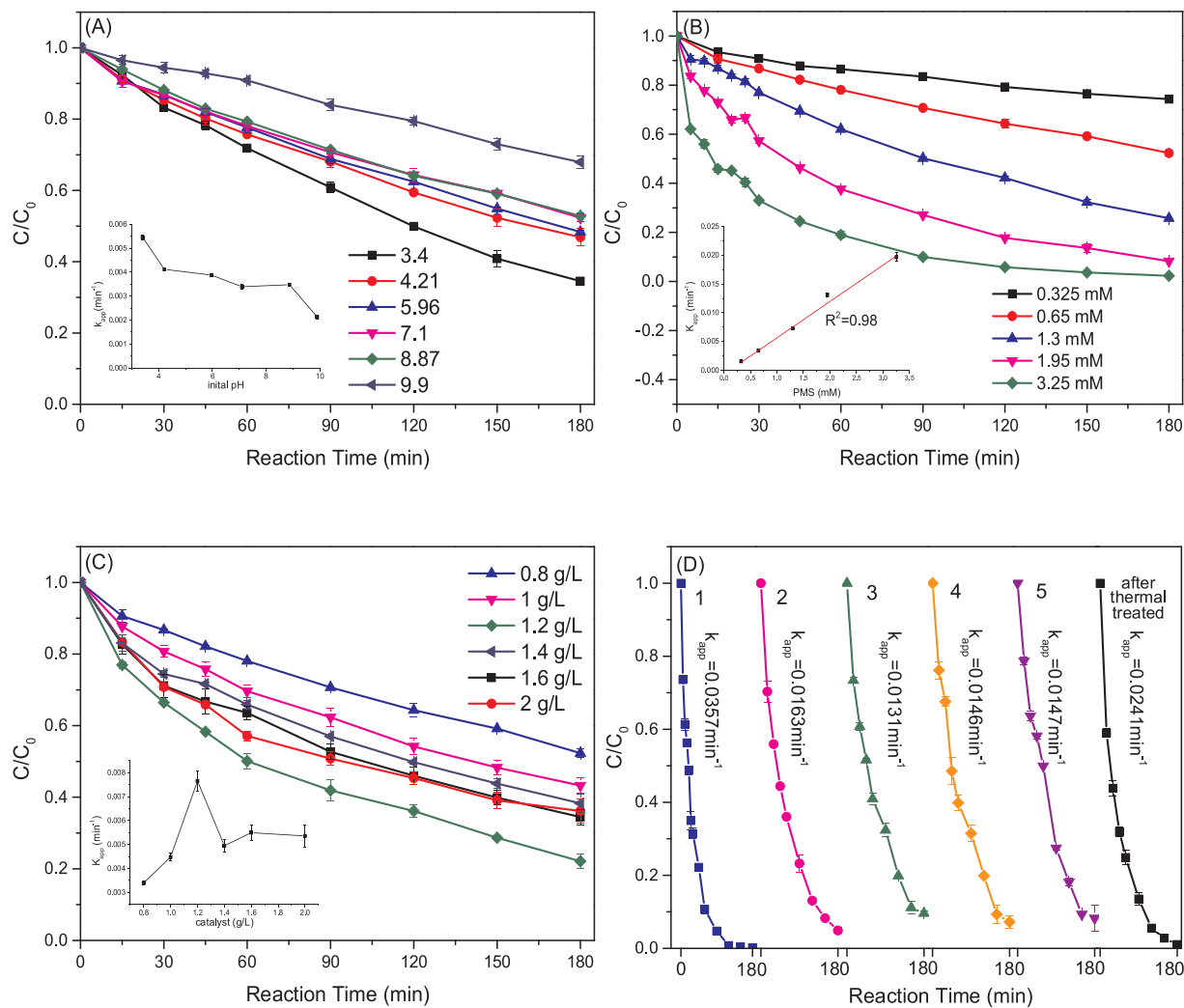


Fig. 5. Effects of (A) reaction initial pH; (B) PMS concentration; (C) catalyst dosage and (D) reuse on RhB degradation in SR-photo-Fenton with C1B2O-5. Reaction condition: [RhB] = 25 mg/L, [PMS] = 0.65 mM, [catalyst] = 0.8 g/L, initial pH = 7.1 and the changes of corresponding parameters were shown in figures (A) (B) and (C); [RhB] = 25 mg/L, [PMS] = 1.95 mM, [catalyst] = 1.2 g/L, initial pH = 7.1 in (D).

citric acid [33], acting as an important reaction site for PMS activation owing to the cycling reaction between Cu(I) and Cu(II). As copper dose increased, the observed intensity of copper peaks increased accordingly. Fig. 3(C) shows XPS spectra of the Bi 4f peak, which contained two individual symmetric peaks at approximately 158.6 and 163.9 eV, with a separation of 5.3 eV, being assigned to Bi 4f_{7/2} and Bi 4f_{5/2}, respectively. This result indicates that bismuth existed in +3 valence states [34]. Fig. 3(D) shows the peaks of O 1s XPS spectra, peaks at 529.7, 531.2, and 533.2 eV were attributed to lattice oxygen (O²⁻), surface hydroxyl groups (−OH), and absorbed water, respectively [35]. By comparing the ratio of the −OH/O²⁻ signals, it was concluded that the interaction between α-Bi₂O₃ and CuBi₂O₄ increased the intensity of surface −OH groups, which are important sites for efficient PMS activation, as previously reported for a Co₃O₄–Bi₂O₃ system [36].

3.2. Performance evaluation

The catalytic activity of the obtained samples in the SR-photo-Fenton was evaluated (Fig. 4). Less than 15% of RhB was oxidized by PMS under visible light irradiation. This was higher than the removal efficiency of PMS or visible light irradiation alone. The SR-photo-Fenton reaction with C1B2O-5 exhibited greater RhB degradation performance (63.6%), compared with SR-Fenton (34.0%) and visible light activation of PMS (12.9%). All the prepared catalysts promoted the

degradation of RhB (Fig. 4(B) (C) and (D)). The value of k_{app} for SR-photo-Fenton was much higher than the sum of that for visible light/PMS and SR-Fenton with C1B2O-5 (Table S1). The synergistic effect on RhB degradation was observed in SR-photo-Fenton reaction with C1B2O-5 as catalyst.

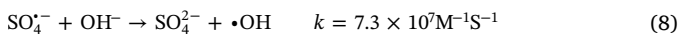
In Fig. 4(B), the removal efficiencies of RhB were 50.5% and 36.9% for C1B2O-7 (pure CuBi₂O₄) and α-Bi₂O₃, respectively. The C1B2O-3 consisting of α-Bi₂O₃, β-Bi₂O₃ and Bi₂O₂CO₃ exhibited better degradation of RhB under visible light irradiation, which is also enhanced by PMS. However, the degradation of RhB was almost stopped in the later 2 h. This may be due to the negative influence on the reactive sites by the surface adsorption of formed intermediates of RhB [37]. The composites of CuBi₂O₄ and α-Bi₂O₃ (as C1B2O-4, C1B2O-5, and C1B2O-6) showed stronger RhB degradation, compared with the pure crystal phase of CuBi₂O₄ or α-Bi₂O₃. The interaction of α-Bi₂O₃ and CuBi₂O₄ increased the surface −OH content, as indicated by the XPS analysis, and led to synergistic effect further. Surface −OH groups have been reported to play a critical role in PMS activation reaction [35]. In the above samples, C1B2O-4 and C1B2O-5 showed the best performance. Based on analysis of XRD, TG-DTA, and FT-IR results, C1B2O-5 showed no nitrate and citrate impurities and was more stable and suitable for water treatment processes. Therefore, 500 °C was selected as the optimum calcination temperature. Additionally, the effects of the molar ratio of Cu/Bi on performance of catalysts calcined at 500 °C are given

in Text S6. It was found that the presence of CuO in the as-prepared composites was good for the development of catalytic activity and this effect was more obvious with the increasing CuO content. More importantly, the pure CuO showed the highest performance and no synergistic effect was observed between CuO and CuBi₂O₄ (Fig. 4(D)). Copper ions leaching was very significant when copper was over doped in precursor (Fig. 4(E)). This result was also reported in literatures [38,39]. Firstly, CuO is unstable in acidic conditions, so the samples with CuO in this study showed significant copper ion dissolution when acidic PMS was added. Secondly, Cu(II) on the surface of solid catalyst would form complexes with PMS, which reduced stability of CuO and thus promoted copper ions release from the solid [38]. The leached [Cu²⁺] increased with the increasing of copper dose (Fig. 4(E)). The leached copper ions (50.0 mg/L) did not make any contribution to PMS activation (Fig. S6), indicating that this was a heterogeneous reaction. But the significant dissolution of Cu²⁺ resulted in toxic copper ion pollution and loss of the active component from the solid catalyst. This was a major problem for the practical application.

The concentration of leached copper ion was very low when an excess of bismuth was used to prepare the catalysts, as for C1B2O-5 (shown in the right part of Fig. 4(E)). When the initial pH varied in the range of 3.4 to 9.9, the leached [Cu²⁺] gradually declined from 0.043 to 0.006 mg/L. The small amount of copper ions that dissolved over a wide range of pH values indicates that the prepared C1B2O-5 is highly stable. This stability could be attributed to the strong interaction between CuBi₂O₄ and α-Bi₂O₃, which led to the as-prepared catalyst showing stable catalytic activity and very low leaching of copper ions. Considering C1B2O-5 showed better performance in activation of PMS for RhB degradation with very lower copper ion leaching, and both nitrate and citrate could be decomposed in the calcination process. C1B2O-5 was selected as the optimized catalyst for further study.

3.3. Effects of initial solution pH, [PMS] and [catalyst]

As shown in Fig. 5(A), the removal of RhB decreased from 65.5% to 53.1% when the initial pH was increased from 3.4 to 4.21. When the initial pH was increased from 4.21 to 8.87, the removal efficiency of RhB and k_{app} (shown in Table S2) remained almost unchanged. However, the removal efficiency decreased apparently to 32.1% when the initial pH was increased to 9.9. The above results indicate that acidic conditions are more favorable for RhB degradation by the SR-photo-Fenton reaction with C1B2O-500. As acidic intermediates formed during the SR-photo-Fenton reaction the solution pH decreased. This decrease became more pronounced when the initial pH was high (Fig. S7). It was reported that the pK_a values of RhB and PMS are 3.0 [40] and 9.4 [41], respectively. Thus, the ionization states of RhB⁻ and HSO₅⁻ did not change over the pH range 3–9. The C1B2O-5 catalyst surface was positively charged over the investigated pH range because the pH_{pzc} value was measured to be approximately 10.9 (Fig. S8). Electrostatic attraction between HSO₅⁻ or RhB⁻ and the positively charged surface –OH groups on C1B2O-5 occurs over the initial pH range 3.4–9.9. This interaction derived the activation PMS reaction, which not be influenced by variation of the initial pH. In acidic solutions, SO₄²⁻ is the main reactive radical formed from the decomposition of PMS. As the initial solution pH increased from acidic to basic, more ·OH were formed, replacing SO₄²⁻ (Eq. (8)).



In neutral or basic pH solution, the redox potentials of ·OH and SO₄²⁻ were 1.9–2.7 V or 2.5–3.1 V, respectively [42]. The lower redox potential of ·OH leads to a decrease of RhB degradation performance as initial solution pH increased. The obvious decrease of k_{app} at pH 9.9 was likely caused by dianion formation of SO₂-5, which has weak oxidizing power and was not able to be activated by catalyst, from PMS under basic conditions [43], according to Eq. (9).



The leached [Cu²⁺] decreased with the increase of initial pH (Fig. 4(E)). Leached Cu²⁺ does not contribute to PMS activation (Fig. S6) but does decrease the catalytic activity of C1B2O-5. The effect of [PMS] and [catalyst] on RhB degradation were also investigated and the results are shown in the Text S7. The optimized reaction conditions were [PMS]₀ = 1.95 mM and [catalyst]₀ = 1.2 g/L. A detailed comparison between as-obtained sample in this study and related catalysts in literatures, was shown in Table S3, indicating that as-prepared α-Bi₂O₃/CuBi₂O₄ in this study showed a stronger catalytic activity for contaminants degradation or oxidant activation under visible light.

3.4. Reusability and regeneration of catalyst

The reusability of C1B2O-5 was evaluated by cycling testing (Fig. 5(D)) under the optimized reaction conditions, including [PMS] and [catalyst] under neutral pH. Samples were separated from the suspension by centrifugation after the first reaction, rinsed with deionized water, and then dried at 60 °C for 8 h for reuse. As shown in Fig. 4(D), the removal efficiency of RhB slightly decreased but over 90% RhB was removed within 3 h in the second-use. However, the value of k_{app} decreased from 0.0357 to 0.0163 min⁻¹ when the catalyst was used for the second time. In following recycles, k_{app} remained stable for up to five cycles. The leaching of Cu²⁺ was less than 0.1 mg/L (Fig. 4(E)), suggesting that leached Cu²⁺ did not cause a decrease in catalyst activity. The activity decrease in the second-use might be attributed to surface adsorption of intermediates formed from RhB degradation, which blocked interactions among the catalyst, PMS and RhB. The adsorbed intermediates could not be removed by the simple water washing process [44]. After adsorption saturation, this interface reaction stabilized, resulting in slight variation of k_{app} for 3 to 5 cycles. The catalyst could be regenerated by calcination according to literature reports [44,45], through combustion of the adsorbed intermediates. Therefore, the C1B2O-5 after five cycling tests was calcined in air at 500 °C for 1 h for reuse. RhB was completely degraded within 2 h, which was almost the same performance as that of the fresh catalyst. After a thermal treatment, the adsorbed intermediates attached on the surface of C1B2O-5 were removed and the catalytic activity of C1B2O-5 could be fully recovered. No notable changes occurred, only the strength of diffraction peaks slightly weakens was observed in XRD spectra of used C1B2O-5 (Fig. S9). The sample regenerated by the thermal treatment showed similar intensity of diffraction peaks as that of the fresh sample. The above results suggested that C1B2O-5 showed relatively stable performance and that calcination was able to clear surface adsorbed intermediates and regenerate the C1B2O-5.

3.5. Identification of reactive oxygen radical (ROS) and intermediates

To identify the reactive radicals, EPR trapping experiments with DMPO as a spin trapping agent were conducted and corresponding results are shown in Fig. 6(A). No characteristic peaks were identified in the EPR spectra from neither PMS nor catalyst alone under visible light irradiation. Strong EPR signals of DMPO-·OH adducts and DMPO-SO₄²⁻ adducts were observed in SR-Photo-Fenton reaction with C1B2O-5 as a catalyst. The appearance of DMPO-·OH ($a_N = 14.9$ G, $a_H = 15.0$ G) and DMPO-SO₄²⁻ (with hyperfine splitting constants of $a_N = 13.2$ G, $a_H = 9.6$ G, $a_H = 1.48$ G and $a_H = 0.78$ G) adducts [46] revealed the presence of both ·OH and SO₄²⁻. EPR experiments were conducted under different pH conditions (Fig. 6(B)), confirming that acidic solution promoted the formation of radical and the increase of [OH⁻] resulted in the transformation of SO₄²⁻ to ·OH (Eq. (8)).

Competitive radical experiments were performed to further investigate the ROS responsible for RhB degradation. It has been widely reported that TBA can be used as an effective scavenger of ·OH, owing to TBA with a very high reaction activity with ·OH

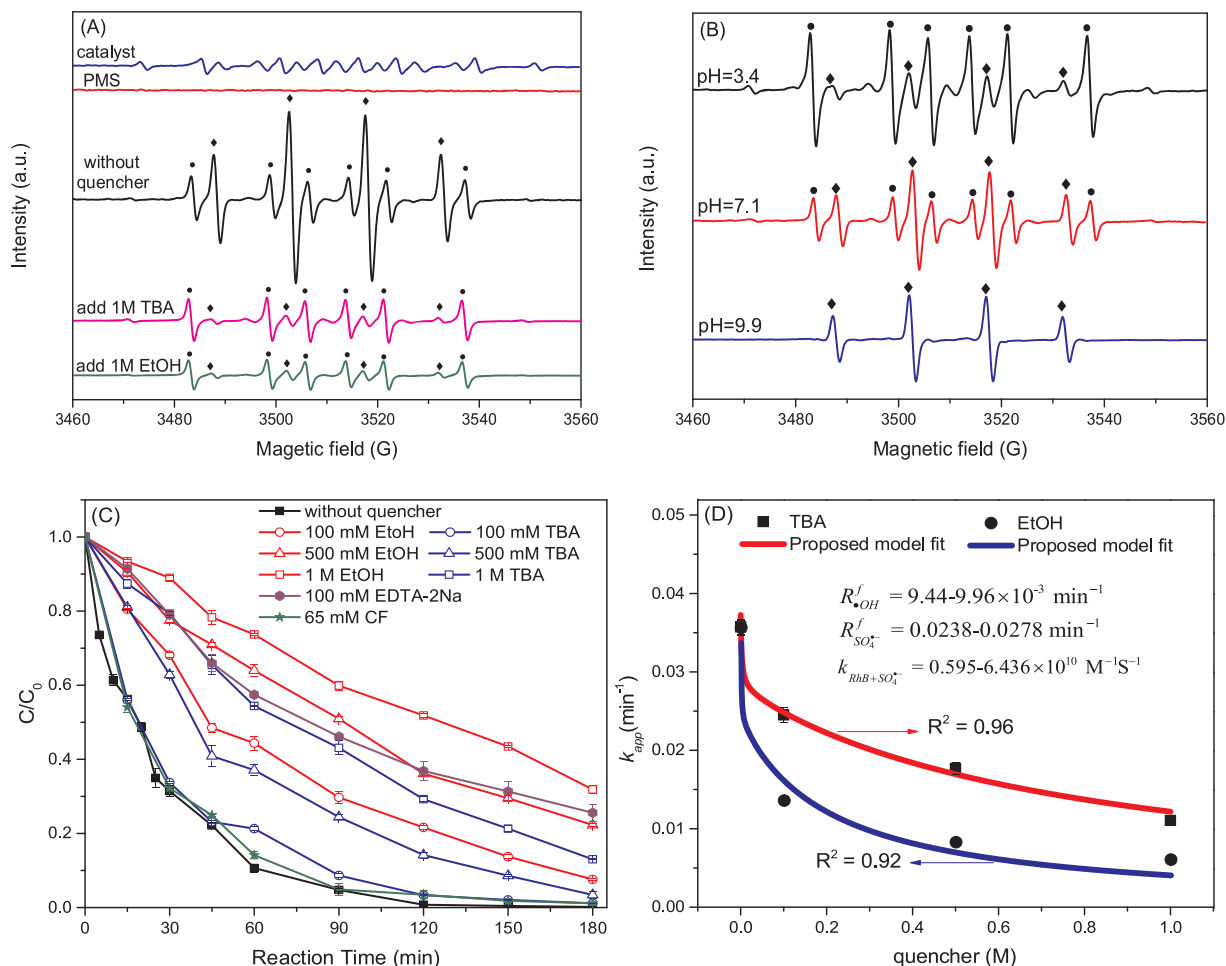


Fig. 6. (A) EPR spectra in various reactions (● DMPO- $\text{SO}_4^{\cdot-}$, ◆ DMPO- $\cdot\text{OH}$); (B) EPR spectra under different initial pH; (C) effects of quencher on RhB degradation and (D) multivariate non-linear fitting between k_{app} with [quencher] Reaction condition: [RhB] = 25 mg/L, [PMS] = 1.95 mM, [catalyst] = 1.2 g/L and initial pH = 7.1; in EPR experiment, RhB was not added.

($k = 6.0 \times 10^8 \text{ M}^{-1}\text{S}^{-1}$) [47], whereas the reaction activity of TBA with $\text{SO}_4^{\cdot-}$ is relative low ($k = 4.0 \times 10^5 \text{ M}^{-1}\text{S}^{-1}$) [48]. Ethanol (EtOH) has been used as an effective quenching reagent for both $\cdot\text{OH}$ ($k = 1.9 \times 10^9 \text{ M}^{-1}\text{S}^{-1}$) [47] and $\text{SO}_4^{\cdot-}$ ($k = 1.6 \times 10^7 \text{ M}^{-1}\text{S}^{-1}$) [48]. The inhibition effects of EtOH and TBA on RhB degradation under neutral pH condition are shown in Fig. 6(C). The removal efficiency of RhB only slightly decreased when 100 mM EtOH or TBA was added to the reaction. The relatively obvious quenching effect was observed until 1 M EtOH or TBA (i.e., at a concentration more than 500 times that of PMS) was added, and the removal efficiency of RhB decreased by 31.8% and 13%, respectively, compared with that of the control experiment. However, the inhibitory effect of such a high concentration of quencher was not notable compared with previous report [23], in which less than 10% of sulfanilamide was degraded when 1.0 mM EtOH was added to the reaction solution. Herein, we propose that surface radicals might be involved in the $\text{CuBi}_2\text{O}_4\text{-Bi}_2\text{O}_3/\text{PMS}$ reaction system. It was consistent with the findings of Lei et al. [49], where it was reported that surface radicals generated from persulfate activated by $\text{CuO-Fe}_3\text{O}_4$ are likely responsible for the destruction of phenol. To verify this speculation, EPR experiment was performed in the presence of 1.0 M EtOH or TBA. It was found that the EPR signals were still observed although the intensity decreased considerably, particularly that of $\cdot\text{OH}$ (Fig. 6(A)). This result might be attributed to alcohols failing to completely capture surface-adsorbed radicals [49,50]. The presence of surface radicals was confirmed by EPR experiments results. In addition, chloroform (CF), a widely recognized scavenger of $\text{O}_2^{\cdot-}$ ($k = 3 \times 10^{10} \text{ M}^{-1}\text{S}^{-1}$) [51], was added to the reaction solution. The negligible inhibition effect

indicated that $\text{O}_2^{\cdot-}$ was not responsible for RhB degradation. To determine the possible role of h^+ generated by visible light irradiation on the photocatalyst [7], EDTA-2Na (100 mM) was added to reaction solution. After that, apparent inhibition effect was observed, suggesting the involvement of photogenerated h^+ in the reaction. However, no photocatalytic reaction was observed in Fig. 4(A), which could be explained by the rapid recombination of photogenerated h^+/e^- . In the presence of PMS, the photogenerated h^+ reacted with PMS to generate $\text{SO}_4^{\cdot-}$ (Eqs. (3) and (4)) [10], which was a photo-assistant reaction. The addition of EDTA-2Na showed a more significant quenching effect than that of EtOH and TBA, suggesting an important role of h^+ in promoting the production of $\text{SO}_4^{\cdot-}$. The competitive radical experiment was also conducted in acidic solution. The quenching effect was worse than that under neutral condition (Fig. S10), indicating that more radicals were formed in acidic solution. This result confirmed that better RhB degradation performance could be achieved under acidic condition owing to the formation more $\text{SO}_4^{\cdot-}$. According to the analysis above, surface-bonded and free radicals including $\text{SO}_4^{\cdot-}$ and $\cdot\text{OH}$ were major ROS and the assistance of visible light was also important for this novel AOP.

A kinetic model to estimate the $\text{SO}_4^{\cdot-}$ and $\cdot\text{OH}$ formation rate was obtained from the results of above competitive radical experiments based on a previous reported kinetic analysis method [51]. Based on the apparent rate constant (k_{app}) of RhB degradation with respect to the amount of added EtOH/TBA, the following kinetic expressions could be obtained as Eqs. (10) and (11) for EtOH or TBA quenching experiments, respectively.

$$\begin{aligned}
k_{app} &= \frac{R_{\cdot OH}^f k_{RhB+\cdot OH}[RhB]}{k_{RhB+\cdot OH}[RhB] + k_{EtOH+\cdot OH}[EtOH]} + \frac{R_{SO_4^{* -}}^f k_{RhB+SO_4^{* -}}[RhB]}{k_{RhB+SO_4^{* -}}[RhB] + k_{EtOH+SO_4^{* -}}[EtOH]} \\
&= \frac{1}{\frac{1}{R_{\cdot OH}^f} + \frac{k_{EtOH+\cdot OH}}{R_{\cdot OH}^f k_{RhB+\cdot OH}}[EtOH]}[EtOH] \\
&\quad + \frac{1}{\frac{1}{R_{SO_4^{* -}}^f} + \frac{k_{EtOH+SO_4^{* -}}}{R_{SO_4^{* -}}^f k_{RhB+SO_4^{* -}}}[EtOH]}[EtOH]
\end{aligned} \tag{10}$$

$$\begin{aligned}
k_{app} &= \frac{R_{\cdot OH}^f k_{RhB+\cdot OH}[RhB]}{k_{RhB+\cdot OH}[RhB] + k_{TBA+\cdot OH}[TBA]} + \frac{R_{SO_4^{* -}}^f k_{RhB+SO_4^{* -}}[RhB]}{k_{RhB+SO_4^{* -}}[RhB] + k_{TBA+SO_4^{* -}}[TBA]} \\
&= \frac{1}{\frac{1}{R_{\cdot OH}^f} + \frac{k_{TBA+\cdot OH}}{R_{\cdot OH}^f k_{RhB+\cdot OH}}[TBA]}[TBA] + \frac{1}{\frac{1}{R_{SO_4^{* -}}^f} + \frac{k_{TBA+SO_4^{* -}}}{R_{SO_4^{* -}}^f k_{RhB+SO_4^{* -}}}[TBA]}[TBA]
\end{aligned} \tag{11}$$

Where $R_{\cdot OH}^f$ and $R_{SO_4^{* -}}^f$ are the formation rate of $\cdot OH$ and $SO_4^{* -}$, respectively; $k_{RhB+\cdot OH}$ and $k_{RhB+SO_4^{* -}}$ are the second-order rate constants for the reaction of RhB with $\cdot OH$ ($k_{RhB+\cdot OH}$ is $0.9\text{--}2.5 \times 10^{10} M^{-1} s^{-1}$ [47]) and $SO_4^{* -}$, respectively; $k_{EtOH+\cdot OH}$ and $k_{EtOH+SO_4^{* -}}$ are the second-order rate constants for the reaction of EtOH with $\cdot OH$ and $SO_4^{* -}$, respectively, which were obtained from previous reports [47,48]; $k_{TBA+\cdot OH}$ and $k_{TBA+SO_4^{* -}}$ are the second-order rate constants for the reaction of TBA with $\cdot OH$ and $SO_4^{* -}$, respectively [47,48]. According to Eqs. (10) or (11), the plots showing the change of k_{app} with [quencher] in Fig. 6(D) were fitted by multivariate non-linear fitting, and the results are shown in Table S4. The second-order rate constant of RhB reacting with $SO_4^{* -}$ was calculated to be $0.595\text{--}6.436 \times 10^{10} M^{-1} s^{-1}$. In addition, the formation rates of $\cdot OH$ and $SO_4^{* -}$ were $0.944\text{--}0.996 \times 10^{-2} min^{-1}$ and $2.38\text{--}2.78 \times 10^{-2} min^{-1}$, respectively. These results indicated that the formation rate of $SO_4^{* -}$ was at least 2.4 times as high as that of $\cdot OH$, and $SO_4^{* -}$ was the dominant ROS for RhB degradation.

Five kinds of RhB degradation intermediates with conjugate xanthene ring structure were identified by HPLC and are shown in Table S5. Variations of these intermediates at different reaction time were measured by peak area from UV detector and are shown in Fig. 7. It was found that the concentrations of *N,N*-diethyl-*N'*-ethylrhodamine (DER), *N*-ethyl-*N'*-ethylrhodamine (EER), *N,N*-diethylrhodamine (DR), neethylrhodamine (ER), and rhodamine (R) increased rapidly then decreased slowly over time. DER formed first and its yield was much higher than other *N*-de-ethylation intermediates, confirming that DER was the first intermediate. DR showed the second highest yield, indicating that $=N(C_2H_5)_2$ was more easily de-ethylated than $=N^+(C_2H_5)_2$. All peaks disappeared from the HPLC chromatograms after

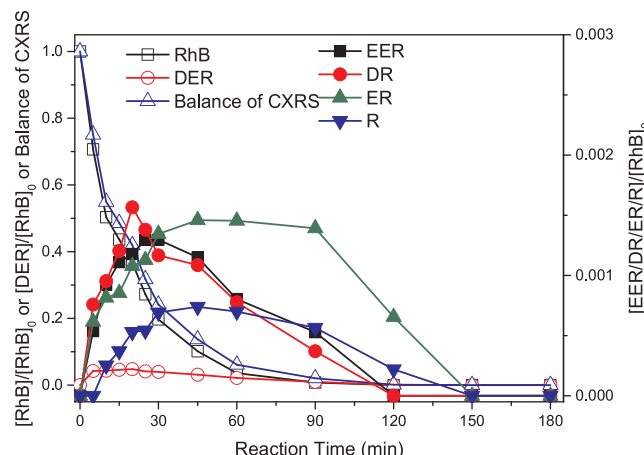


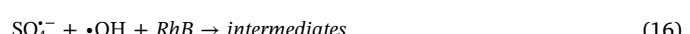
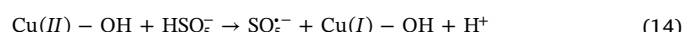
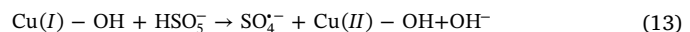
Fig. 7. Profile of intermediates and RhB in SR-photo-Fenton. Reaction condition: [RhB] = 25 mg/L, [PMS] = 1.95 mM, [catalyst] = 1.2 g/L and initial pH = 7.1.

150 min, indicating that intermediates containing conjugate xanthene ring structure (CXRS) were completely degraded. Based on the structural information, RhB and all the detected intermediates contained CXRS. The imbalance of CXRS (Fig. 7), indicated that ring opening intermediates were formed at higher concentrations than the detected intermediates. The residual TOC estimated from RhB and *N*-de-ethylated intermediates was compared with that determined by TOC analyzer, and the results are shown in Fig. S11. The removal efficiency of TOC reached to 67% after 180 min, and the residual TOC may be ascribed to a large number of recalcitrant ring-opened intermediates and small molecule products. This was also confirmed by the imbalance of TOC results based identified intermediates.

3.6. Proposed reaction mechanism

XPS spectra of fresh and used C1B2O-5 are shown in Fig. S12. The position of peaks corresponding to Bi 4f_{7/2} and Bi 4f_{5/2} did not change following the reaction, indicating that Bi remained +3 valence states and was not involved in PMS activation. Peaks corresponding to Cu 2p_{3/2} were observed at 935.5 and 932.4 eV for Cu²⁺ and Cu⁺, respectively. According to the peak areas of Cu²⁺ and Cu⁺, the ratio of Cu⁺/Cu²⁺ was 0.16 after the reaction, which was higher than that of fresh catalyst (0.10). The above results indicate that cycling of Cu⁺/Cu²⁺ occurred during the reaction [32] and more active Cu⁺ formed through reduction by photogenerated e⁻. The O 1s XPS spectra indicate that the ratio of –OH/O²⁻ changed from 2.58 to 0.86 after the reaction, suggesting the involvement of surface –OH in the catalytic reaction [52].

Based on the competitive radical experiments, EPR experiments, and XPS analysis, a mechanism of SR-photo-Fenton reaction with C1B2O-5 as catalyst can be proposed. When C1B2O-5 is irradiated by visible light, electron-hole pairs are generated, as detailed in Eq. (12). However, recombination of e⁻ and h⁺ is rapid, resulted in no direct photocatalytic reaction (Fig. 4(A)). In the presence of PMS, e⁻ and h⁺ could react with PMS to generate SO₄^{·-} and ·OH (Eqs. (3)–(6)). This reaction partly inhibited the re-combination of e⁻ and h⁺. Additionally, Cu(I)-OH on the C1B2O-5 surface promotes the decomposition of PMS to produce SO₄^{·-}, accompanied with the oxidation to Cu (II)-OH (Eq. (13)). The presence of Bi₂O₃ promotes the formation of surface –OH groups on the obtained catalyst and is better than bismuth in CuBi₂O₄. The Cu(I)-OH could be regenerated via the reaction between the formed Cu(II)-OH and PMS (Eq. (14)). What's more, the presence of photo-generated e⁻ could reduce Cu(II)-OH to Cu(I)-OH (Eq. (13)), which facilitates the cycling of Cu(I)/Cu(II). The e⁻ transformation accelerates the generation of SO₄^{·-}. The transfer of e⁻/h⁺ and cycling of Cu(I)/Cu(II) facilitate the effective activation of PMS to generate SO₄^{·-} and ·OH. The formed free radicals are responsible for the degradation of RhB in this SR-photo-Fenton reaction with assistance of visible light. The above described reaction occurred on the surface of C1B2O-5. PMS could be decomposed to generate SO₄^{·-} and ·OH by visible light irradiation in solution (Eq. (7)). Finally, the combination of surface and solution reactions led to the formation of SO₄^{·-} and ·OH, which resulted in degradation of RhB (Eq. (16)).



4. Conclusion

In this study, CuBi₂O₄ and its composites with α-Bi₂O₃ or CuO were

prepared by a simple sol-gel method and applied to RhB degradation in a SR-photo-Fenton reaction. The calcination temperature and molar ratio of Cu:Bi showed notable effects on the crystal phase composition and morphology, leading to different performance of the SR-photo-Fenton reaction. The optimized catalyst was synthesized with calcination at 500 °C and a Bi:Cu molar ratio of 2.0, which showed the best activity and less copper ion leaching. Calcination at 500 °C was an optional method for CuBi₂O₄ composites regeneration. The roles of h⁺, SO₄²⁻ and ·OH were identified by competitive radical and EPR experiments. The reaction mechanism was proposed that the transfer of e⁻/h⁺ and cycling of Cu(I)/Cu(II) facilitate the effective activation of PMS to generate SO₄²⁻ and ·OH under the assistance of visible light. At last, we used a simple radical competition kinetic method to calculate the reaction rate constant of RhB with SO₄²⁻ and estimate the formation rate of ·OH and SO₄²⁻. The latter one was the main ROS in this reported SR-photo-Fenton.

Acknowledgements

This work was performed with the support of the Fundamental Research Funds for the Central Universities (No. 2017PT01), the National Natural Science Foundation of China (Nos. 51578520 and 51378063), and Beijing Natural Science Foundation (No. L160006).

Appendix A. Supplementary data

Supplementary material related to this article can be found, in the online version, at doi:<https://doi.org/10.1016/j.apcatb.2018.04.058>.

References

- [1] C. Cai, H. Zhang, X. Zhong, L. Hou, J. Hazard. Mater. 283 (2015) 70–79.
- [2] Y. Wang, Y. Xie, H. Sun, J. Xiao, H. Cao, S. Wang, J. Hazard. Mater. 301 (2016) 56–64.
- [3] Y. Pang, H. Lei, Chem. Eng. J. 287 (2016) 585–592.
- [4] W.D. Oh, Z. Dong, T.-T. Lim, Appl. Catal. B: Environ. 194 (2016) 169–201.
- [5] Q. Chen, F. Ji, Q. Guo, J. Fan, X. Xu, J. Environ. Sci.—China 26 (2014) 2440–2450.
- [6] Y. Liu, H. Guo, Y. Zhang, W. Tang, X. Cheng, H. Liu, Chem. Phys. Lett. 653 (2016) 101–107.
- [7] Y. Wang, X. Zhao, D. Cao, Y. Wang, Y. Zhu, Appl. Catal. B: Environ. 211 (2017) 79–88.
- [8] F. Wu, H. Huang, T. Xu, W. Lu, N. Li, W. Chen, Appl. Catal. B: Environ. 218 (2017) 230–239.
- [9] R. Sharma, V. Kumar, S. Bansal, S. Singhal, J. Mol. Catal. A: Chem. 402 (2015) 53–63.
- [10] K.Y.A. Lin, Z.Y. Zhang, Sep. Purif. Technol. 173 (2017) 72–79.
- [11] M. Ahmadi, F. Ghanbari, M. Moradi, Water Sci. Technol. 72 (2015) 2095–2102.
- [12] A.M. Abdulkareem, J. Li, A.A. Aref, L. Ren, E.M. Elssfah, H. Wang, Y. Ge, Y. Yu, Mater. Res. Bull. 46 (2011) 1443–1450.
- [13] Y. Xie, Y. Zhang, G. Yang, C. Liu, J. Wang, Mater. Lett. 107 (2013) 291–294.
- [14] W. Shi, F. Guo, S. Yuan, Appl. Catal. B: Environ. 209 (2017) 720–728.
- [15] M. Nishikawa, S. Yuto, T. Hasegawa, W. Shiroishi, H. Honghao, Y. Nakabayashi, Y. Nosaka, N. Saito, Mater. Sci. Semicond. Process. 57 (2017) 12–17.
- [16] L. Wei, C. Shifu, Z. Huaye, Y. Xiaoling, J. Exp. Nanosci. 6 (2011) 102–120.
- [17] M. Nishikawa, S. Hiura, Y. Mitani, Y. Nosaka, J. Photochem. Photobiol. A 262 (2013) 52–56.
- [18] A. Muthukrishnaraj, S. Vadivel, I.M. Joni, N. Balasubramanian, Ceram. Int. 41 (2015) 6164–6168.
- [19] M. Chen, Q. Yang, L. Li, M. Liu, P. Xiao, M. Zhang, Mater. Lett. 171 (2016) 255–258.
- [20] Y. Zhang, Y. Xie, J. Li, T. Bai, J. Wang, J. Sol-Gel Sci. Technol. 71 (2014) 38–42.
- [21] Y. Zhang, Y. Xie, J. Li, G. Yang, T. Bai, J. Wang, J. Alloys Compd. 580 (2013) 172–175.
- [22] W.D. Oh, S.K. Lua, Z. Dong, T.T. Lim, Nanoscale 7 (2015) 8149–8158.
- [23] W.D. Oh, Z. Dong, T.T. Lim, Catal. Today 280 (2017) 2–7.
- [24] W.D. Oh, S.K. Lua, Z. Dong, T.T. Lim, Nanoscale 8 (2016) 2046–2054.
- [25] Y. Wang, F. Li, T. Xue, C. Liu, D. Yuan, F. Qi, B. Xu, Environ. Sci. Pollut. Res. 25 (2018) 4419–4434.
- [26] W.D. Oh, Z. Dong, Z.T. Hu, T.T. Lim, J. Mater. Chem. A 3 (2015) 22208–22217.
- [27] W. Shan, Y. Hu, Z. Bai, M. Zheng, C. Wei, Appl. Catal. B: Environ. 188 (2016) 1–12.
- [28] M.K. Hossain, G.F. Samu, K. Gandhi, S. Santhanagopalan, J.P. Liu, C. Janáky, K. Rajeshwar, J. Phys. Chem. C 121 (2017) 8252–8261.
- [29] J. Zhang, Y. Jiang, W. Gao, H. Hao, J. Mater. Sci.-Mater. Electron. 26 (2014) 1866–1873.
- [30] J. Hou, C. Yang, Z. Wang, W. Zhou, S. Jiao, H. Zhu, Appl. Catal. B: Environ. 142–143 (2013) 504–511.
- [31] R. Patil, S. Kelkar, R. Naphade, S. Ogale, J. Mater. Chem. A 2 (2014) 3661–3668.
- [32] Y. Zhang, C. Liu, B. Xu, F. Qi, W. Chu, Appl. Catal. B: Environ. 199 (2016) 447–457.
- [33] L. Zhang, L. Lyu, Y. Nie, C. Hu, Sep. Purif. Technol. 157 (2016) 203–208.
- [34] K. Brezesinski, R. Ostermann, P. Hartmann, J. Perlich, T. Brezesinski, Chem. Mater. 22 (2010) 3079–3085.
- [35] X. Pang, Y. Guo, Y. Zhang, B. Xu, F. Qi, Chem. Eng. J. 304 (2016) 897–907.
- [36] Y. Ding, L. Zhu, A. Huang, X. Zhao, X. Zhang, H. Tang, Catal. Sci. Technol. 2 (2012) 1977.
- [37] Q.S. Wu, Y. Cui, L.-M. Yang, G.Y. Zhang, D.Z. Gao, Sep. Purif. Technol. 142 (2015) 168–175.
- [38] T. Zhang, H. Zhu, J.P. Croue, Environ. Sci. Technol. 47 (2013) 2784–2791.
- [39] X. Du, Y. Zhang, I. Hussain, S. Huang, W. Huang, Chem. Eng. J. 313 (2017) 1023–1032.
- [40] D.V.T. Kasnavia, D.A. Sabatini, Ground Water 37 (1999) 376–381.
- [41] Y.H. Guan, J. Ma, X.C. Li, J.Y. Fang, L.W. Chen, Environ. Sci. Technol. 45 (2011) 9308–9314.
- [42] F. Ghanbari, M. Moradi, Chem. Eng. J. 310 (2017) 41–62.
- [43] T. Zeng, M. Yu, H. Zhang, Z. He, J. Chen, S. Song, Catal. Sci. Technol. 7 (2017) 396–404.
- [44] Y. Wang, H. Sun, H.M. Ang, M.O. Tadé, S. Wang, Chem. Eng. J. 245 (2014) 1–9.
- [45] X. Duan, H. Sun, J. Kang, Y. Wang, S. Indrawirawan, S. Wang, ACS Catal. 5 (2015) 4629–4636.
- [46] Y. Wang, H. Sun, H.M. Ang, M.O. Tade, S. Wang, ACS Appl. Mater. Interface 6 (2014) 19914–19923.
- [47] G.V. Buxton, C.L. Greestock, W.P. Helman, A.B. Ross, J. Phys. Chem. Ref. Data 17 (1988) 513–886.
- [48] P. Neta, R.E. Huie, A.B. Ross, U.S. Dept. of Commerce, National Bureau of Standards 17 (1979) 1027–1284.
- [49] Y. Lei, C.S. Chen, Y.J. Tu, Y.H. Huang, H. Zhang, Environ. Sci. Technol. 49 (2015) 6838–6845.
- [50] Y. Yao, C. Lian, Y. Hu, J. Zhang, M. Gao, Y. Zhang, S. Wang, J. Hazard. Mater. 338 (2017) 265–275.
- [51] W. Huang, M. Brigante, F. Wu, C. Mousty, K. Hanna, G. Mailhot, Environ. Sci. Technol. 47 (2013) 1952–1959.
- [52] Y. Ren, L. Lin, J. Ma, J. Yang, J. Feng, Z. Fan, Appl. Catal. B: Environ. 165 (2015) 572–578.